Characterization of the Atlantic Water and Levantine Intermediate Water in the Mediterranean Sea using 20 years of Argo Data

Fedele Giusy[1,*], Mauri Elena [1], Notarstefano Giulio [1] and Poulain Pierre Marie[1]

(1) National Institute of Oceanography and Applied Geophysics, OGS, 34010 Sgonico (TS), Italy

* Corresponding author (gfedele@inogs.it)

The Atlantic Water (AW) and Levantine Intermediate Water (LIW) are important water masses that play a crucial role in the internal variability of the Mediterranean thermohaline circulation. In particular, their variability and interaction, along with other water masses that characterize the Mediterranean basin, such as the Western Mediterranean Deep Water (WMDW), contribute to modify the Mediterranean Outflow through the Gibraltar Strait and hence may influence the stability of the global thermohaline circulation.

This work aims to characterize the AW and LIW in the Mediterranean Sea, taking advantage of the large observational dataset provided by Argo floats from 2001 to 2019. Using different diagnostics, the AW and LIW were identified, highlighting the inter-basin variability and the strong zonal gradient that denote the two water masses in this marginal sea. Their temporal variability was also investigated in the last two-decades, providing a more robust view of the AW and LIW characteristics, which in previous studies, due to lack of data, have been investigated taking advantage of very short periods.

A clear salinification and warming trend characterize the AW and LIW in the last two decades (~0.007 ± 0.140 and 0.006 ± 0.038 yr^{-1}; 0.026 ± 0.715 and 0.022 ± 0.232 °C yr^{-1}, respectively). The salinity and temperature trends found at subbasin scale are in good agreement with previous results. The strongest trends are found in the Adriatic basin in both the AW and LIW properties. A subbasin dependent spectral variability emerges in the AW and LIW salinity timeseries with peaks between 2 and 10 years.

1   Introduction

The Atlantic Water (AW) and Levantine Intermediate Water (LIW) play a central role in the internal variability of the Mediterranean thermohaline circulation, contributing to the dense water formation in this enclosed basin (Tsimplis et al., 2006). The variability and interaction of these two water masses modulate the Mediterranean outflow through the Gibraltar Strait, which plays an important role on the North Atlantic oceanic variability, and in turn to the stability of the global thermohaline circulation (e.g., Rahmstorf, 2006; Hernandez-Molina et al., 2014). Therefore, from a climatic point of view, it is relevant to characterize their main properties and monitor their variability, which are the main purpose of this paper.

Flowing in the Mediterranean Sea through the Gibraltar strait, the AW is less dense than the surrounding water masses and therefore it populates most of the Mediterranean surface layer. Its path is mainly driven by the Coriolis effect and by the complex topography that characterizes this region (Millot and Taupier-Letage 2005).

The LIW is the most voluminous water mass produced in the Mediterranean Sea (e.g., Skliris 2014; Lascaratos et al., 1993), and the saltiest water formed with a relatively high temperature at intermediate depths. It is formed in the Levantine subbasin, after which it is named, where one of the main formation sites is the Rhodes Gyre (e.g., Tsimplis et al., 2006; Kubin et al., 2019). The LIW strongly influences the thermohaline circulation, flowing at intermediate depths and then passing over the sills, exiting the Gibraltar Strait and modifying the Atlantic circulation (Rahmstorf, 1998; Bethoux et al., 1999).

53   Several studies have been devoted to the analysis of the AW and LIW main features and

54   variability, taking advantage of different indicators to identify and track these two water masses

55   in the Mediterranean Sea. Among them, the AW and the LIW are usually referred to the minimum

56   and maximum salinity in the surface and intermediate layers of the water column, respectively

57   (e.g., Millot and Taupier-Letage 2005; Bergamasco and Malanotte-Rizzoli, 2010; Mauri et al.,

58   2019; Juza et al., 2019; Kokkini et al., 2019; Várgas-Yañez et al., 2020). However, different

59   approaches can also be found in the literature. In particular Millot (2014) associated the LIW to

60   the maximum of the potential temperature vertical gradient found in an intermediate water layer,

61   while Bosse et al. (2015) identified the LIW in the northwestern Mediterranean Sea with the

62   maximum salinity value found between two potential density values ($\sigma_\theta = [29.03 - 29.10]\frac{kg}{m^3}$),

63   encompassing both temperature and salinity maxima characterizing the LIW layer. The main

64   findings related to the hydrological properties of these two water masses are summarized below.

65   The AW enters in the Mediterranean Sea through the Gibraltar Strait, occupying the upper 200

66   m of depth with potential density, temperature and salinity annual mean values: $\sigma_\theta \cong$

67    $[26.5 - 27]\frac{kg}{m^3}, T \cong [14 - 16]°C, S \cong [36.0 - 36.5]$ respectively (e.g., Bergamasco and

68   Malanotte-Rizzoli, 2010; Hayes et al., 2019). The AW flowing at the surface, continuously

69   interacts with the atmosphere and is subject to evaporation and mixing with the underlying water

70   masses. Flowing eastward, it becomes denser and the minimum salinity core sinks. Therefore, it

71   can be capped by the surface mixed layer and less influenced by air-sea interactions. Its properties

72   and variability are also modified by the local eddies and by the river discharges in the coastal

73   regions. These mechanisms shape the AW, leading to an increase of salinity from about 36.25 in

74   the Gibraltar Strait to values around 39.2 in the Levantine Sea (e.g., Bergamasco and Malanotte-

75   Rizzoli, 2010; Hayes et al., 2019). These values highlight strong AW temperature and salinity

76   gradients between the Western Mediterranean (WMED) and the Eastern Mediterranean (EMED).

77   The properties of the LIW core in the WMED are commonly referred to the following ranges

78   of potential density, temperature, salinity and depth, respectively: $\sigma_\theta = [29 - 29.10]\frac{kg}{m^3}, T =$

79    $[13 - 14.2]°C, S = [38.4 - 38.8], D = [200 - 600]m$ (e.g. Millot, 2013; Hayes et al., 2019;

80   Várgas-Yañez et al., 2020); while in the EMED these properties span over different values: $\sigma_\theta =$

81    $[28.85 - 29.15]\frac{kg}{m^3}, T = [14.6 - 16.4]°C, S = [38.85 - 39.15], D = [150 - 400]m$ (e.g.

82   Lascaratos et al., 1993; Hayes et al., 2019). Therefore, moving westward, T and S decrease and

83   the LIW sinks.

84   These studies provide a general view of the AW and LIW properties in the Mediterranean Sea,

85   highlighting a strong inter-basin variability of these water masses along their paths, which in turn

86   influences their temporal changes.

87   An example is given by a recent paper by Kassis and Korres (2020), which provides a detailed

88   view of the EMED hydrographic properties for the period 2004–2017 taking advantage of Argo

89   data. Exploring the water column from the surface down to 1500 m in seven different regions of

90   the EMED, they revealed a high inter-annual variability of the stored heat and salt over this region.

91   In this study, following a similar approach, we investigate the AW and LIW properties,

92   isolating their main characteristics and variability from the surrounding water masses, taking

93   advantage of several diagnostics discussed in section 2.2. Our work aims to provide a more robust

94   view of the AW and LIW characteristics, which in previous studies, due to lack of data, have been

95   investigated taking advantage of short periods.

96   In the frame of climate change studies, it is important to estimate possible impacts of AW and

97   LIW changes on the Mediterranean climate, since this region is one of the most vulnerable climate

98   change hotspots (Giorgi 2006). In fact, changes in temperature and salinity can strongly affect the

99   marine system over the Mediterranean and related human activities.

100   Previous studies highlighted a clear salinification of the Mediterranean Sea over the past few

101   decades (e.g., Painter and Tsimplis 2003; Vargas -Yáñez et al., 2010; Schroeder et al., 2017;

102   Skliris et al., 2018) and a clear deep water warming trend after 1980s, which in literature is often

103   related to the Nile River damming and to the global warming (Vargas-Yáñez et al., 2010). Positive

104   temperature and salinity trends, oscillating between [0.0016÷0.0091] °C/yr and [0.0008÷0.001]

105   yr[-1], respectively, are found in the deep layer (below ~700 meters) between 1950 to 2005 (e.g.,

106   Bethoux et al., 1990; Rohling and Bryden, 1992; Millot et al., 2006; Vargas-Yáñez et al., 2010;

107   Borghini et al., 2014).

This observed salinification and warming are also found at intermediate depths in several studies (e.g., Zu et al., 2014; Schroeder et al., 2017; Skliris et al., 2018), with ranges that depend on the region of investigation. A clear positive salinity trend between 150-600 m is found in the Mediterranean Sea by Skliris et al. (2018), analyzing the MEDATLAS data from 1950 to 2002 ($\sim 0.007 \pm 0.004$ yr^{-1}).

In contrast, heterogeneous temperature trends are found in the upper layer in different regions (Painter and Tsimplis, 2003). This sensitivity of the trends to the area of interest, can be due to several reasons, such as the changes in the large-scale atmospheric forcing of the Mediterranean region, the river runoff which differ from one region to another, and to the data coverage over a specific area (e.g., Painter and Tsimplis, 2003; Vargas -Yáñez et al., 2009; 2010). In this respect, Vargas -Yáñez et al. (2009) highlighted that the scarcity of data makes trend estimations very sensitive to the data postprocessing, comparing results from different studies dealing with the same time period. Therefore, in order to reduce the uncertainty of the trend estimations, longer and less sparse timeseries are needed.

In this respect, this work aims to provide an updated view of the temporal evolution and trends of the AW and LIW, taking advantage of the large observational dataset provided by the MedArgo Program (Poulain et al., 2007). It covers the water column from the surface down to ~2000 m over the entire Mediterranean basin from 2001 to 2019. The Mediterranean Sea has been widely studied through the deployment of hundreds of Argo profiling floats (Argo 2020) in the last two decades as part of various national, European and international programs (Wong et al., 2021) and with the participation of different institutions. For these reasons, this dataset constitutes an optimal observational framework to investigate the AW and LIW properties.

The dataset and the methods used in this study are described in section 2, the results are presented in section 3, where the inter-basin and inter-annual variabilities of the AW and LIW in the Mediterranean Sea are shown. The main conclusions are drawn in section 4.

2   Data and method

2.1   Data

In this work the AW and LIW properties in the Mediterranean Sea are investigated taking advantage of the Argo float dataset, which consists of more than thirty thousand T-S profiles for the period 2001–2019. Since 2001, the number of observations is generally increasing, reaching a peak of 4188 profiles in 2015, mainly thanks to the combined efforts of national and international Argo initiatives. The deployments of most Argo floats in the Mediterranean were coordinated by the MedArgo regional center (Poulain et al., 2007). In the Mediterranean, the cycling period is usually reduced to 5 days, and the maximum profiling depth is mostly 700 or 2000 m (Poulain et al., 2007). The floats are equipped with Sea-Bird Conductivity-Temperature-Depth (CTD) sensors (model SBE41CP; www.seabird.com/sbe-41-argo-ctd/product-details?id=54627907875) with accuracies of ±0.002° C, ±0.002 and ±2 dbar for temperature, salinity and pressure, respectively. The data measured by the profilers are transmitted to satellites (e.g., via the Iridium or Argos telemetry systems), then to ground receiving stations, processed and real-time quality-controlled by the Argo Data Assembly Centres (https://www.euro-argo.eu/Activities/Data-Management/Euro-Argo-Data-Centres), sent to the Global Data Assembly Center and made available for free to users (https://fleetmonitoring.euro-argo.eu/dashboard?Status=Active). The delayed-mode quality control applied on pressure, temperature and salinity follows the guidelines described in the Argo Quality Control Manual for CTD (e.g., Wong et al., 2021; Cabanes et al., 2016), in conjunction with other procedures developed at regional level (Notarstefano and Poulain, 2008; Notarstefano and Poulain, 2013) to check the salinity data and any potential drift of the conductivity sensor.

The analyses are performed in eight Mediterranean sub-basins following the climatological areas defined by the EU/MEDARMEDATLAS II project (http://nettuno.ogs.trieste.it/medar/climatologies/medz.html), emphasizing the processes that take place in each sub-basin and modify the water mass properties. Fig. 1 shows the geographical distribution of the Argo profiles from 2001 to 2019 in the eight sub-basins considered (Algerian, Catalan, Ligurian, Tyrrhenian, Adriatic, Ionian, Cretan and Levantine). The Alboran, Aegean and the Sicily Channel sub-basins are not analyzed in this work due to the scarcity of observations in these areas.

164   Most sub-basins are well spatially covered, except for the Adriatic Sea, where the majority of

165   observations are concentrated in the South Adriatic Pit (SAP) and therefore it is important to keep

166   in mind that the results found for this region, are representative of the southern Adriatic Sea. The

167   SAP is an important deep water convection site in the Mediterranean Sea (e.g., Kokkini et al.,

168   2019; Mauri et al., 2021, Azzaro et al., 2012; Bensi et al., 2013) and therefore it is also considered

169   as a crucial area from a climatic perspective. The temporal distribution of the float data is different

170   in the various sub-basins: the longest time series are available in the Ionian, Cretan and Levantine

171   regions, with data from 2001 to 2019, followed by the Algerian, Ligurian and Tyrrhenian sub-

172   basins where data are available after 2003, and then by the Adriatic Sea with data only after 2009.

173   In this context, it is important to mention that the low density in space and time of the Argo

174   profiles induces uncertainties in the results, especially during the first years of the analyzed

175   period.

176

177   **2.2 Methods**

178   As discussed in the introduction, many indicators/characteristics have been adopted in

179   literature to track the AW and LIW in the Mediterranean Sea. Most of them consider, as best

180   indicator, the minimum/maximum salinity at surface/intermediate layer for the AW/LIW and

181   motivated us to follow a similar approach (e.g., Millot and Taupier-Letage, 2005; Bergamasco

182   and Malanotte-Rizzoli, 2010; Hayes et al., 2019; Lamer et al., 2019).

183   A preliminary step in this analysis was the post-processing: we first applied a time sub-

184   sampling on each profiler to obtain a more homogeneous dataset (Notarstefano and Poulain,

185   2009). This is applied to each float as follows: if the cycling period is 1 day or less, the profiles

186   are sub-sampled every 5 days; if the period is 2 or 3 days, they are sub-sampled every 6 days; and

187   if the period is 5 or 10 days, no subsampling is applied. Afterward, each profile was linearly

188   interpolated from the surface (0 m) to the bottom every 10 m to obtain comparable profiles; and

189   finally, a running filter with a 20 m window, was applied to the data along the depth axis, to

190   smooth any residual spike.

191 Finally, the minimum/maximum salinity value in each profile is associated to the AW/LIW

192 core in the respective depth layer. Then, the correspondent depth and temperature values are

193 considered.

194 Once the AW and LIW core are identified in each profile, the AW and LIW inter-basin

195 variabilities were analyzed taking advantage of the boxplot approach applied to each parameter

196 and region (Fig. 2). In Fig.2, the whiskers (black dashed line out of the box) extend to the most

197 extreme data points not considering the outliers at the 5% significance level ($pvalue \leq 0.05$). In

198 order to test the significance, the Student's t distribution was applied to each hydrological

199 parameter in every sub-basin (Kreyszig and Erwin 1970). The null hypothesis (that states that the

200 population is normally distributed) is rejected with a 5% level of statistical significance. This

201 method is also applied to the timeseries trends. In section 3.1 we often refer to the range and

202 skewness of the distributions, that are the difference between the upper and lower limits and the

203 measure of the symmetry of the distributions, respectively (including only the 5% significance

204 values).

205 Considering only the AW/LIW salinity, temperature, and depth values at 95% level of

206 significance (Fig.2), as done for the spatial analysis, the timeseries from 2001 to 2019 have been

207 computed in each subbasin to analyze the low frequency variability (LFV) and trends at

208 interannual to decadal timescale over the available observed periods. In this respect, the high

209 frequency variability was filtered out, first by subtracting the mean seasonal cycle to the raw

210 timeseries, and then applying a median yearly average filter. This last step is needed since the

211 data are not homogeneous in time in every subbasin from 2001 to 2019, and therefore without it,

212 the seasonal variability can contaminate the estimation of the trends. The latter have been

213 computed using the linear least-squares method to fit a linear regression model to the data.

214

215 **3   Results and discussion**

216 In this section, the AW and LIW properties are investigated in the eight Mediterranean climatic

217 regions before mentioned, focusing both on their spatial and temporal variability. The analysis of

218 the trends and spectral features are also shown.

219

3.1 Inter-basin variability

(i)   AW

The hydrological properties of the AW core in eight sub-basins (Fig. 1) are shown in Figs. 2a, b, c, providing a compact view of the AW inter-basin variability for each parameter using the boxplot approach.

Moving eastward, the AW salinity increases from ~36 to 39.5 (minimum and maximum whiskers limits; Fig. 2a), since the surface salinity minimum is progressively smoothed by horizontal mixing with surrounding saltier waters. In fact, as discussed by Font et al. (1998) the AW minimum salinity is dependent on the different degrees of mixing due to its residence times.

In the Algerian sub-basin, the salinity range reaches the highest extension compared to the other regions, probably due to the large baroclinic instability that produces high mesoscale variability in the surface layer and horizontal mixing by strong eddies (Demirov and Pinardi 2007).

The AW salinity range is smaller in the Catalan, Ligurian and Tyrrhenian Seas, where similar distributions are found both in terms of range and skewness (which is close to zero): the main mode and the median have salinity of ~38. In the Adriatic Sea the distribution is probably skewed toward higher values because a clear positive salinity trend is found (Fig. 3; Lipizer et al., 2014). In the Adriatic, Ionian and Cretan Seas, the range is higher than the surrounding sub-basins: in the Adriatic and Ionian Sea this could be associated to the Bimodal Oscillation System (BiOS), and then to the reversal of the North Ionian Gyre (Rubino et al., 2020), while in the Cretan Sea we speculate that it is caused by the sinking of the AW during winter. This is in agreement with Schroeder (2019), where it is shown that in the Cretan Sea, the strong wind-induced evaporation and heat loss during winter lead the AW transformation into salty and warm Cretan Intermediate Water. The depths reached in the Cretan basin (Fig. 2c) seem to confirm this hypothesis.

The AW temperature is highly variable, ranging between ~5 and ~30 °C, with a wider range in the Catalan and Adriatic regions (Fig. 2b), possibly due to the higher seasonal sea surface temperature variability over these sub-basins (Shaltout and Omstedt 2014). The lowest

9

247 temperatures detected can be related to the freshwater fluxes in these regions. In this respect, an

248 episode that can be relevant for the AW distribution in the Adriatic Sea is the large river runoff

249 observed in 2014 by Kokkini et al. (2019), which caused a saline stratification for more than a

250 year. This episode is also captured by our analyses (Fig. 3). As observed for the AW salinity

251 mode, even the temperature mode shift toward higher values moving eastward in agreement with

252 the literature (Bergamasco and Malanotte-Rizzoli 2010). In the Algerian basin the AW

253 temperature mode is higher than it is in the Catalan subbasin: this can be due to the influence of

254 freshwater fluxes in the Catalan region and led by the high eddy activity over the Algerian region

255 (Escudier et al., 2016) led by the strong baroclinic instability already discussed for the salinity

256 field (e.g., Demirov and Pinardi 2007; Cotroneo et al., 2016; Aulicino et al., 2018; Aulicino et al.,

257 2019). The temperature and salinity ranges captured in the Algerian region are in good agreement

258 with those found by Cotroneo et al. (2020) and shown in their Table 2.

259 The depths of the AW core oscillate between 0 and 90 m with the main mode sinking eastward

260 (Fig. 2c). The distributions are all skewed toward lower depths, with the maximum probability

261 density function (PDF) near surface and a median shifting from 0 to 45 m moving eastward,

262 indicating a clear sinking of the AW along its pathway.

263

264 (ii)   LIW

265 In this section, the main hydrological properties of the LIW are analyzed in each sub-basin.

266 Flowing away from the region of formation, the LIW interacts with the surrounding water

267 masses and becomes less salty; the salinity sharply drops from ~39.2 to ~38.5, moving from the

268 Levantine to the Ligurian subbasin, and then it becomes more stable in the Algerian and Catalan

269 regions, oscillating around ~38.5 (Fig.2e). The distributions are highly symmetric around the

270 median and the variability decreases flowing westward maybe because the LIW becomes deeper,

271 sinking from ~100 to ~650 m (Fig. 2g). The highest salinity is reached in the Cretan basin, where

272 the formation of salty and warm Cretan Intermediate Water, caused by strong wind-induced

273 evaporation and heat loss during winter, influences the LIW properties and detection (Schroeder,

274 2019).

275 The LIW temperature decreases westward from ~18 to ~12.8 °C. The range is higher in the

276 EMED as also found for salinity, suggesting that over this region, the intrusion of warmer and

277 saltier surface waters due to convective processes characterizes the LIW formation (Fig. 2f;

278 Schroeder, 2019).

279 The sinking of the LIW flowing westward is shown in Fig. 2g, dropping from about 100 to

280 650 m (maximum whiskers values). The distributions tend to be symmetric in most of the

281 Mediterranean Sea, except for the Adriatic Sea, where a strong LIW bimodality in the depth

282 domain is found (in agreement with Kokkini et al., 2019), with two peaks located at ~190 and

283 ~500 m respectively (here not shown); this behavior explains the big range that characterizes this

284 region. The investigation of the Adriatic bimodality is beyond the scope of this paper.

285

286 **3.2 Interannual variability**

287 In this section, the temporal variability of the AW and LIW in each sub-basin is studied

288 analyzing the 1-year moving average timeseries and the relative trends.

289 The results of this analysis are affected by the irregular spatial and temporal sampling of the

290 Argo floats. Time gaps in the data are found in the Catalan, Tyrrhenian and Cretan Seas (Fig. 3).

291 The missing data are due to the lack of Argo float samplings. Data in the Adriatic Sea are available

292 only after 2009, while the Ionian, Cretan and Levantine sub-basins have much longer timeseries,

293 with data covering the period from 2001 to 2019.

294

295 **3.2.1 Trends**

296 (i) AW trends

297 The AW salinity temporal evolution is shown in Fig. 3, where significant trends (at 5% level of

298 significance) are found in each region (Table 1). Positive trends are clearly found in the EMED

299 and in the Tyrrhenian Sea, highlighting a clear salinification of the AW in the last two decades

300 over most of the Mediterranean Sea (~0.007±0.140 yr^{-1}; Table 1). Comparable positive salinity

301 trends between 0-150 m (~0.009±0.009 yr^{-1}) are also found in Skliris et al. (2018) where multi-

11

302   decadal salinity changes in the Mediterranean Sea are investigated taking advantage of the

303   MEDATLAS database (MEDAR Group 2002) consisting of temperature and salinity profiles in

304   the   Mediterranean   from   1945   to   2002

305   (https://www.bodc.ac.uk/resources/inventories/edmed/report/4651/). A clear meridional

306   separation is found in the AW trends during the observed period. In the Tyrrhenian Sea and in the

307   entire EMED the AW becomes saltier, with significant positive trends, whilst in the WMED, a

308   significant negative trend emerges in the Algerian and Catalan subbasins (Table 1). This

309   freshening of the AW inflow could be related to the observed rapid freshening of the North

310   Atlantic Ocean (Dickson et al. 2002), which causes are related to different phenomenon, included

311   the accelerating Greenland melting triggered by the global warming (Dukhovskoy et al., 2019).

312   These findings seem in contradiction with the results provided by Millot (2007), showing a

313   salinification of the Mediterranean outflow, obtained analyzing autonomous CTDs on the

314   Moroccan shelf in the strait of Gibraltar in the period 2003-2007, which may be caused by the

315   different epochs under study. In fact, comparing Fig. 3 in Millot (2007) and Fig. 3 in this work, a

316   similar positive trend is captured in the Algerian sub-basin, in the same period; while extending

317   the analysis to a longer timeseries, a clear negative trend leads the AW variability at interannual

318   to decadal timescale. Opposite trends are found in the EMED and in the Tyrrhenian subbasin,

319   where the very strong increase in net evaporation of ~8 to 12% over 1950-2010 (Skiliris et al.,

320   2018) and the damning of the Nile River (as projected by Nof, 1979) may have caused the AW

321   salinification. The trends are steep in the Adriatic and Cretan sub-basins, where the salinity

322   increases with an order of magnitude higher ($O[10^{-2}]$) and the largest increase is found in the

323   Adriatic Sea ($0.044\pm0.188\ yr^{-1}$). Here the impact of the negative E-P anomalies and large river

324   runoff observed by Kokkini et al. (2019) around 2014 is well captured by the salinity time series.

325   The results in the EMED are in good agreement with Fig. 9 of Kassis and Korres (2020), where

326   the yearly average salinity per depth zone and per region between 2004-2017 are shown.

327   Similarities in the observed trend in the Ionian Sea ($0.009 \pm 0.181\ yr^{-1}$) are also found by Zu

328   et al., 2014 (mean trend~$0.011\ yr^{-1}$), where the Argo floats data between 2004 and 2014 are

329   analyzed.

According to the above-mentioned meridional salinity transition from negative to positive salinity trends moving eastward, the temperatures also show a meridional shift from positive to negative significant trends east of the Ionian Sea, with a mean positive AW temperature trend over the eight analyzed sub-basins (0.026 ±0.715 °C/yr; Table 1). Interbasin changes between the subbasins are instead linked to changes in the large-scale meteorological forcing of the Mediterranean region (Painter and Tsimplis, 2003). As found for the salinity field, the sharper increase is related to the Adriatic Sea (~0.117±0.951 °C/year), highlighting the presence of mechanisms that enhance the trends over this region. A sharpening in the trend over the last decade is captured in the Catalan subbasin (Fig.7) and confirmed by Schuckmann et al. (2019), who observed the same behavior in the Northwestern Mediterranean with a trend over the last decade (~0.047 °C/yr), that doubles the respective trend in the previous 1982-2011 period (0.029 °C/yr).

The AW depths time series (Fig. 5) show a heterogeneous trend in the Mediterranean Sea, with significant negative values (the depth decreases) in the Algerian and Ionian subbasins, and positive in the Tyrrhenian and Levantine regions (Table 1), which reflects into a tendency of the AW to become shallower, increasing the stratification at basin scale (0.238±10.537 m/yr). Wider temporal changes are found in the Levantine region, where the trend is from one to two orders of magnitude higher than the other regions.

(ii)   LIW

The LIW temporal variability is hereafter analyzed. Fig. 6 shows the salinity changes from 2001 to 2019 in the eight subbasins considered. A positive trend is found in the whole Mediterranean Sea at 5% level of significance, highlighting a salinification also at intermediate depths of this enclosed basin over two decades (~0.006 ±0.038 yr^{-1}; Table 1). A similar positive trend between 150-600 m is found by Skliris et al. (2018), in the MEDATLAS data from 1950 to 2002 (~0.007±0.004 yr^{-1}), with lower standard deviations. The higher standard deviations found in this study, compared to those founds by Skliris et al. (2018) could be related to the wider range of depths considered and to the different epochs considered. The LIW properties vary less than

13

the AW in most of the basin, except for the Ligurian, and Levantine regions, where deep water and LIW water formations occur respectively. The strongest salinity increase is found in the Adriatic Sea (0.021 ± 0.074 yr^{-1}), exceeding the trends in other regions by one order of magnitude.

The LIW salinity positive trends over the Mediterranean Sea are also found by Zu et al. (2014), which confirms the salinification of the basin at intermediate depths, as also observed at surface in most of the analyzed regions. This suggests that the enhancement of the net evaporation over the Mediterranean in the last decades, that was observed by Skiliris et al. (2018), may lead the formation of saltier LIW in the EMED, and as consequence a mean positive salinity trend over the whole basin. While, in the WMED, positive trends (0.008 ± 0.002; 0.009 ± 0.0007 yr^{-1}; from gliders missions) are found from 2011 to 2017 by Juza et al. (2019), in agreement with the positive trends found in the last few years in the western subbasins shown in Fig.6.

Positive temperature trends (5% level of significance) are found in the whole Mediterranean Sea except in the Cretan sub-basin where the LIW becomes colder with no significance values (Fig. 7). Oscillations with decadal timescales overlaps the warming trend in the Cretan and Levantine sub-basins and matches the low frequency signal captured by the correspondent salinity timeseries. This is confirmed by the continuous wavelet transforms applied to the timeseries (not shown). Peaks of salinity and temperature are observed in ~2009 in the Levantine basin and then reach the Cretan Sea in ~2010. The same variability is discussed in Ozer et al. (2017) and explained in connection with the Ionian Bimodal Oscillating System (BiOS). These maxima are in fact attributed to periods of anticyclonic circulation in the north Ionian (2006-2009) and limited AW advection to the south-eastern Levantine basin, referring to the study by Artale et al. (2006). The LIW temperature mean trend and standard deviation averaged over the eight subbasins are ~0.002 $\pm$0.232 °C/yr (Table 1), which can be interpreted as a weaker response of the intermediate layers to the warming trend observed at surface.

The sub-basins with the steepest increase are located in the central longitudinal band of the Mediterranean Sea, therefore far from the LIW main sources. The range of temperature and salinity and the respective variability in the Tyrrhenian and Ionian sub-basins are in good agreement with Poulain et al. (2009), where T and S timeseries from 2001 to 2009 are computed

14

386   from Argo floats data near 600 m. The ranges and trends for T and S found in the Ligurian Sea

387   are also confirmed by Margirier et al. (2020), where vertical profiles collected by gliders, Argo

388   floats, CTDs and XBTs in the northwestern Mediterranean Sea over the 2007–2017 period are

389   analyzed.

390   The LIW depth time series are shown in Fig. 8: significant negative trends (the depth

391   decreases) are found in the Tyrrhenian, Ionian, and Cretan Seas, while in the Catalan and

392   Levantine sub-basins the LIW sinks ($pvalue \leq 0.05$). Non-significant trends are found in the

393   other regions. Abrupt shifts are found in the Adriatic sub-basin from ~200 m to ~500-600 m at

394   different time steps (trend ~2.609$\pm$115.404 m/yr), highlighting a bimodal behavior of the LIW

395   depth and an intense dense water production activity as also shown by Kokkini et al. (2019).

396   Previous studies attribute dramatic shifts in the Adriatic hydrological properties to the BiOS and

397   the Eastern Mediterranean Transient (e.g., Vilibić et al., 2012). This hypothesis can also be

398   supported by correlations between the BiOS (definition by Vilibić et al., 2020) and the AW/LIW

399   salinity yearly averaged timeseries in the Adriatic Sea, which maximum values are about -0.49/-

400   0.43 at lag 0 /-4 yr (at negative year lag, the BiOS leads; $pvalue \leq 0.05$). Further investigations

401   are left to future studies.

402   The results related to the EMED match those shown in Kassis and Korres (2020), where the

403   timeseries of salinity and temperature averaged between different depths-layers (below 100 m) in

404   similar subbasins are shown (see Fig. 8 in Kassis and Korres 2020). The LIW depth mean trend

405   and standard deviation averaged over the eight subbasins is 1.099$\pm$46.458 m/yr (Table 1).

406

407   **4 Conclusions**

408   We presented an analysis of the main properties and variability of the AW and LIW in the

409   Mediterranean Sea, exploiting the Argo float data that provide an optimal observational dataset

410   to study their thermohaline properties. Indeed, this dataset covers the water column down to

411   ~2000 m and provide data for almost two decades.

412   Taking advantage of different diagnostics discussed in section 2, the AW and LIW have been

413   detected in the Mediterranean Sea through a sub-basin approach, which allowed to define the

414   main hydrological features over this enclosed basin in different regions.

415   In addition to previous studies, this work provides a more detailed view of the AW and LIW

416   characteristics in the last two-decades over most of the Mediterranean Sea, except for the Alboran

417   sub-basin, the Sicily Channel, and the Aegean sub-basin where Argo data are too scarce.

418   To achieve this goal, the first step of this study was the detection of the AW and LIW cores in

419   each available profile. In agreement with previous studies (e.g., Lascaratos et al., 1993;

420   Bergamasco and Malanotte-Rizzoli, 2010; Millot, 2013; Hayes et al., 2019; Várgas-Yañez et al.,

421   2020), we confirmed the mean zonal gradients of the AW and LIW properties over the

422   Mediterranean Sea: the AW becomes saltier, warmer, and deeper moving eastward, while the

423   LIW becomes fresher, colder, and deeper moving westward. These results not only match the

424   present literature but also provide a more detailed view of these water masses over eight sub-

425   basins.

426   The timeseries derived from the AW and LIW parameters have also highlighted some

427   interesting features that are in good agreement with the previous literature. The most relevant

428   results are summarized below:

429   - Positive salinity and temperature trends characterize the AW and LIW in the last two

430   decades over most of the Mediterranean Sea (average value over the whole region:

431   0.007 and 0.006 yr^{-1}; 0.026 and 0.022 °C/yr respectively). The warming and

432   salinification of the Mediterranean Sea is in good agreement with previous results

433   (e.g., Skliris et al., 2018; Margirier et al., 2020; Kassis and Korres, 2020).

434   - Negative AW salinity trends in the Algerian and Catalan sub-basins suggest a

435   freshening of the AW inflow, in agreement with the observed rapid freshening of the

436   North Atlantic Ocean (Dickson et al., 2002).

437   - Positive AW salinity trends are found east of the Ligurian sub-basin, highlighting a

438   clear salinification of this water mass in the last two decades probably due to the

combined effect of the strong increase in net evaporation and the Nile dumming (e.g., Nof, 1979; Skiliris et al., 2018; section 3.2.1a).

- Positive trends in the LIW salinity timeseries are found in the whole Mediterranean Sea at 5% level of significance, highlighting a salinification also at intermediate depths (section 3.2.1b).

- Positive LIW temperature trends ($pvalue \leq 0.05$) are found everywhere except in the Cretan sub-basin where the negative trend is not significant. This highlights a clear warming at intermediate depth of the Mediterranean Sea.

- The AW and LIW depth trends are highly space-dependent, showing different behaviors in the eight sub-basins.

- Abrupt shifts in the LIW depth are found in the Adriatic sub-basin from ~200 m to ~500-600 m at different time steps (trend 2.609±115.404 m/yr), highlighting a bimodal behavior of the LIW depth and an intense dense water production activity as also shown by Kokkini et al. (2019).

These results therefore provide interesting new insights about the AW and LIW interbasin and interannual variability, that can be further analyzed to investigate which mechanisms lead to the observed temporal trends in each sub-basin.

References

Argo: Argo float data and metadata from Global Data Assembly Centre (Argo GDAC). SEANOE. https://doi.org/10.17882/42182, 2020.

Artale V., Calmante S., Malanotte-Rizzoli P., Pisacane G., Rupolo V., and Tsimplis M., In: Lionello, P., Malanotte-Rizzoli, P., Boscoli, R. (Eds.), The Atlantic and Mediterranean Sea as connected systems, in Mediterranean Climate Variability Dev. Earth Environ. Sci. 4. Elsevier, Amsterdam, pp. 283–323, 2006.

Aulicino G., Cotroneo Y., Ruiz S., Sánchez Román A., Pascual A., Fusco G., Tintoré J. and Budillon G.: Monitoring the Algerian Basin through glider observations, satellite altimetry and numerical simulations along a SARAL/AltiKa track. Journal of Marine Systems, 179(), 55–71.doi:10.1016/j.jmarsys.2017.11.006, 2018

Aulicino G., Cotroneo Y., Olmedo E., Cesarano C., Fusco G., and Budillon G.: In Situ and Satellite Sea Surface Salinity in the Algerian Basin Observed through ABACUS Glider Measurements and BEC SMOS Regional Products. Remote Sensing, 11(11), 1361–.doi:10.3390/rs1111136, 2019.

Azzaro M., La Ferla R., Maimone G., Monticelli L.S., Zaccone R., and Civitarese G.: Prokaryotic dynamics and heterotrophic metabolism in a deep convection site of Eastern Mediterranean Sea (the Southern Adriatic Pit), Continental Shelf Research, Volume 44 2012, Pages 106-118, ISSN 0278-4343, https://doi.org/10.1016/j.csr.2011.07.011, 2012.

Bensi M., Cardin V., Rubino A., Notarstefano G., and Poulain P.M.: Effects of winter convection on the deep layer of the Southern Adriatic Sea in 2012, *J. Geophys. Res. Oceans* 118, 6064– 6075, https://doi.org/10.1002/2013JC009432, 2013.

484

485 Bergamasco A., and Malanotte-Rizzoli P.: The circulation of the Mediterranean Sea: A historical

486 review of experimental investigations. Adv. Oceanogr. Limnol. 2010 1 11–28;

487 https://doi.org/10.1080/19475721.2010.491656, 2010.

488

489 Berkowitz J., and Kilian L.: Recent developments in bootstrapping time series. Econometr Rev

490 19:1–48, https://doi.org/10.1080/07474930008800457, 2000.

491

492 Borghini M., Bryden H., Schroeder K., Sparnocchia S., and Vetrano A.: The Mediterranean is

493 becoming saltier, Ocean Sci. 10, 693–700, https://doi.org/10.5194/os-10-693-2014, 2014.

494

495 Bosse A., Testor P., Mortier L., Prieur L., Taillandier V., d'Ortenzio F., and Coppola L.:

496 Spreading of Levantine Intermediate Waters by submesoscale coherent vortices in the

497 northwestern Mediterranean Sea as observed with gliders. Journal of Geophysical Research.

498 Oceans, Wiley-Blackwell 2015 120 (3), pp.1599-1622,

499 https://doi.org/10.1002/2014JC010263, 2015.

500

501 Bethoux J.P., Gentili B., Raunet J., and Taillez D.: Warming trend in the Western Mediterranean

502 deep water. Nature 347, 660–662, https://doi.org/10.1038/347660a0, 1990.

503

504 Bethoux J. P., Gentili B., Morin P., Nicolas E., Pierre C., and Ruiz-Pino D.: The Mediterranean

505 Sea: A miniature ocean for climatic and environmental studies and a key for the climatic

506 functioning of the North Atlantic, *Prog. Oceanogr.*, **44**, 131– 146, doi:10.1016/S0079-

507 6611(99)00023-3, 1999.

508

509 Cabanes C., Thierry V., and Lagadec C.: Improvement of bias detection in Argo float conductivity

510 sensors and its application in the North Atlantic. Deep Sea Research Part I: Oceanographic

511 Research Papers 114 128-136, https://doi.org/10.1016/j.dsr.2016.05.007, 2016.

512

513 Cotroneo Y., Aulicino G., Ruiz S., Pascual A., Budillon G., Fusco G., and Tintoré J.: Glider and

514   satellite high resolution monitoring of a mesoscale eddy in the algerian basin: Effects on the

515   mixed layer depth and biochemistry, Journal of Marine Systems, Volume 162, Pages 73-88,

516   ISSN 0924-7963, https://doi.org/10.1016/j.jmarsys.2015.12.004, 2016.

517

518 Cotroneo Y., Aulicino G., Ruiz S., Sánchez Román A., Torner Tomàs M., Pascual A., Fusco G.,

519   Heslop E., Tintoré J., and Budillon G.: Glider data collected during the Algerian Basin

520   Circulation Unmanned Survey, Earth Syst. Sci. Data, 11, 147–161,

521   https://doi.org/10.5194/essd-11-147-2019, 2019.

522

523 Demirov E. K., and Pinardi N.: On the relationship between the water mass pathways and eddy

524   variability in the Western Mediterranean Sea, *J. Geophys. Res.* 112, C02024,

525   https://doi.org/10.1029/2005JC003174, 2007.

526

527 Dickson B., Yashayaev I., Meincke J., Turrell B., Dye S., and Holfort J.: Rapid freshening of the

528   deep North Atlantic Ocean over the past four decades. *Nature* **416,** 832–837,

529   https://doi.org/10.1038/416832a, 2002.

530

531 Dukhovskoy D.S., Yashayaev I., Proshutinsky A., Bamber J. L., Bashmachnikov I.

532   L., Chassignet E. P., Lee C.M., and Tedstone A.J.: Role of Greenland freshwater anomaly in

533   the recent freshening of the subpolar North Atlantic. *Journal of Geophysical Research:*

534   *Oceans*, 124, 3333– 3360. https://doi.org/10.1029/2018JC014686, 2019.

535

536 Escudier R., Mourre B., Juza M., and Tintoré J.: Subsurface circulation and mesoscale variability

537   in the Algerian subbasin from altimeter-derived eddy trajectories, J. Geophys.Res. Oceans

538   121, 6310–6322, https://doi.org/10.1002/2016JC011760, 2016.

539

540 Font J., Millot C., Pérez JDJS, Julià A., and Chic O.: The drift of Modified Atlantic Water from

541 the Alboran Sea to the eastern Mediterranean. Scientia Marina. 62. 211-216,

542 https://doi.org/10.3989/scimar.1998.62n3211, 1998.

543

544 Giorgi F.: Climate change hot-spots. Geophysical Research Letters, 33: L08707,

545 https://doi.org/10.1029/2006GL025734, 2006.

546

547 Hayes D. R., Schroeder K., Poulain P.M., Testor P., Mortier L., Bosse, A., Du Madron X.: Review

548 of the Circulation and Characteristics of Intermediate Water Masses of the

549 Mediterranean: Implications for Cold-Water Coral Habitats. In: Orejas C., Jiménez C.

550 (eds) Mediterranean Cold-Water Corals: Past, Present and Future. Coral Reefs of the

551 World, vol 9. Springer, Cham, https://doi.org/10.1007/978-3-319-91608-8_18, 2019.

552

553 Hernández-Molina F., Stow D., Zarikian C., Acton G., Bahr A., Balestra B., Ducassou E., Flood

554 R., Flores J.A., Furota S., Grunert P., Hodell D., Jiménez-Espejo F., Kim J.K., Krissek L.,

555 Kuroda J., Li B., Llave E., Lofi J., and Xuan C.: Onset of Mediterranean outflow into the North

556 Atlantic. Science. 344, https://doi.org/10.1126/science.1251306, 2014.

557

558 Juza M., Escudier R., Vargas-Yáñez M., Mourre B., Heslop E., Allen J., and Tintoré J.:

559 Characterization of changes in Western Intermediate water properties enabled by an

560 innovative geometry-based detection approach. Journal of Marine Systems 191, 1–12. doi:

561 10.1016/j.jmarsys.2018.11.003, 2019.

562

563 Kassis D., and Korres G.: Hydrography of the Eastern Mediterranean basin derived from argo

564 floats profile data, Deep Sea Research Part II: Topical Studies in Oceanography, Volume

565 171,2020,104712,ISSN 0967-0645, https://doi.org/10.1016/j.dsr2.2019.104712, 2020.

566

567   Kokkini Z., Mauri M., Gerin R., Poulain P.M., Simoncelli S., and Notarstefano G.: On the salinity

568   structure in the South Adriatic as derived from float and glider observations in 2013–2016,

569   Deep Sea Research Part II: Topical Studies in Oceanography,Volume 171 2020 104625, ISSN

570   0967-0645, https://doi.org/10.1016/j.dsr2.2019.07.013, 2019.

571

572   Kreyszig E.: Introductory Mathematical Statistics: Principles and Methods. New York: Wiley,

573   1970.

574

575   Kubin E., Poulain P.M, Mauri E., Menna M., and Notarstefano G.: Levantine Intermediate and

576   Levantine Deep Water Formation: An Argo Float Study from 2001 to 2017,

577   https://doi.org/10.3390/w11091781, 2019.

578

579   Lamer P.A., Mauri E., Notarstefano G., and Poulain P.M.: The Levantine Intermediate Water in

580   the eastern Mediterranean Sea; http://maos.inogs.it/pub/REPORT_LAMER_final_last.pdf,

581   2019.

582

583   Lascaratos A., Williams R.G., and Tragou E.: A mixed-layer study of the formation of Levantine

584   intermediate water. Journal of Geophysical Research 98, https://doi.org/10.1029/93JC00912,

585   1993.

586

587   Lipizer M., Partescano E., Rabitti A., Giorgetti A., and Crise A.: Qualified temperature, salinity

588   and dissolved oxygen climatologies in a changing Adriatic Sea, Ocean Sci., 10, 771–797,

589   https://doi.org/10.5194/os-10-771-2014, 2014.

590

591   Malanotte-Rizzoli P., Manca B., Marullo S., Ribera d'Alcala M., Roether W., Theocharis A.,

592   Bergamasco A., Budillon G., Sansone E., Civitarese G., Conversano F., Gertman I., Hernt B,

593   Kress N., Kioroglou S., Kontoyiannis H., Nittis K., Klein B., Lascaratos A., and Kovacevic

594   V.: The Levantine Intermediate Water Experiment (LIWEX) Group: Levantine basin—A

595   laboratory for multiple water mass formation processes. Journal of Geophysical Research. 108.

596   8101, https://doi.org/10.1029/2002JC001643, 2003.

597

598   Margirier F., Testor P., Heslop E., Mallil K., Bosse A., Houpert L., Mortier L., Bouin M.-

599   N., Coppola L., D'Ortenzio F., de Madron X.D., Mourre B., Prieur L., Raimbault P., and

600   Taillandier V.: Abrupt warming and salinification of intermediate waters interplays with

601   decline of deep convection in the Northwestern Mediterranean Sea. Sci Rep 10 20923,

602   https://doi.org/10.1038/s41598-020-77859-5, 2020.

603

604   Mauri E., Sitz L., Gerin R., Poulain P.M., Hayes D., and Gildor H.: On the Variability of the

605   Circulation and Water Mass Properties in the Eastern Levantine Sea between September 2016–

606   August 2017. *Water* **2019**, *11*, 1741, https://doi.org/10.3390/w11091741, 2019.

607

608   Mauri E., Menna M., Garić R., Batistić M., Libralato S., Notarstefano G., Martellucci R., Gerin

609   R., Pirro A., Hure M., Poulain P-M, 2021. Recent changes of the salinity distribution and

610   zooplankton community in the South Adriatic Pit, accepted in OSR5.

611

612   Millot C., and Taupier-Letage I.: Circulation in the Mediterranean Sea: Updated description and

613   schemas of the circulation of the water masses in the whole Mediterranean Sea. A. Saliot. The

614   Mediterranean Sea, The Mediterranean Sea (5-K), Springer, pp.29-66 2005, Handbook of

615   Environmental Chemistry, 9783540314929 9783540250180.ff10.1007/b107143ff. ffhal-

616   01191856v1f, https://doi.org/10.1007/b107143, 2005.

617

618   Millot C., Candela J., Fuda J.L., and Tber Y.: Large warming and salinification of the
619   Mediterranean outflow due to changes in its composition. Deep-Sea Res. 53, 656–665,
620   https://doi.org/10.1016/j.dsr.2005.12.017, 2006.

621

622   Millot C.: Interannual salinification of the Mediterranean inflow, Geophys. Res. Lett., 34,
623   L21609, doi:10.1029/2007GL031179, 2007.

624

625   Millot C.: Levantine Intermediate Water characteristics: An astounding general
626   misunderstanding. Scientia Marina. 78, https://doi.org/10.3989/scimar.04045.30H, 2013.

627

628   Millot C.: Levantine intermediate water characteristics: an astounding general misunderstanding!
629   (addendum). Sci. Marina, 78 165-171, https://doi.org/10.3989/scimar.04045.30H, 2014.

630

631   Nof D.: On man-induced variations in the circulation of the Mediterranean Sea. Tellus 31, 558–
632   564, 1979.

633

634   Notarstefano G., and Poulain P. M.: Delayed mode quality control of Argo floats salinity data in
635   the Tyrrhenian Sea. Technical Report OGS 2008/125 OGA 43 SIRE,
636   http://nettuno.ogs.trieste.it/sire/DMQC/dmqc_1900593_54073_V1.pdf, 2008.

637

638 Notarstefano G., and Poulain P. M.: Thermohaline variability in the Mediterranean and Black

639   Seas as observed by Argo floats in 2000-2009. OGS Tech. Rep. OGS 2009/121 OGA 26 SIRE,

640   72 pp.-171, http://dx.doi.org/10.3989/scimar.04045.30H, 2009.

641

642 Notarstefano G., and Poulain P.M.: Delayed mode quality control of Argo salinity data in the

643   Mediterranean Sea: A regional approach. Technical Report OGS 2013/103 Sez. OCE 40

644   MAOS, 2013.

645

646 Ozer T., Gertman I., Kress N., Silverman J., and Herut B.: Interannual thermohaline (1979–2014)

647   and nutrient (2002–2014) dynamics in the Levantine surface and intermediate water masses,

648   SE Mediterranean Sea. Global and Planetary Change, 151, 60–67.

649   doi:10.1016/j.gloplacha.2016.04.001, 2017.

650

651 Painter S.C., and Tsimplis M.N.: Temperature and salinity trends in the upper waters of the

652   Mediterranean Sea as determined from the MEDATLAS dataset, Continental Shelf Research,

653   Volume 23, Issue 16 2003, Pages 1507-1522, ISSN 0278-4343,

654   https://doi.org/10.1016/j.csr.2003.08.008, 2003.

655

656 Poulain P.M., Barbanti R., Font J., Cruzado A., Millot C., Gertman I., Griffa A., Molcard A.,

657   Rupolo V., Le Bras S., and Petit de la Villeon L.: MedArgo: a drifting profiler program in the

658   Mediterranean Sea. Ocean Science, European Geosciences Union 2007, 3 (3), pp.379- 395.

659   hal-00331145, https://doi.org/10.5194/osd-3-1901-2006, 2007.

660

661 Poulain P.M., Solari M., Notarstefano G., and Rupolo V.: Assessment of the Argo sampling in

662 the Mediterranean and Black Seas (part II).

663 http://maos.inogs.it/pub/2009_report_task4.4_partII.pdf, 2009.

664

665 Rahmstorf S.: Influence of Mediterranean Outflow on climate, *Eos Trans. AGU*, **79**, 281– 282,

666 doi:10.1029/98EO00208, 1998.

667

668 Rahmstorf, S.: Thermohaline Ocean Circulation. In: Encyclopedia of Quaternary Sciences, Edited

669 by S. A. Elias. Elsevier, Amsterdam, http://www.pik-

670 potsdam.de/~stefan/Publications/Book_chapters/rahmstorf_eqs_2006.pdf, 2006.

671

672 Roemmich D., Johnson G., Riser S., Davis R., Gilson J., Owens W., Garzoli S., Schmid C., and

673 Mark I.: The Argo Program Observing the Global Ocean with Profiling Floats. Oceanography.

674 22, https://doi.org/10.5670/oceanog.2009.36, 2009.

675

676 Rohling E.J., and Bryden H.L.: Man induced salinity and temperature increase in the Western

677 Mediterranean Deep Water. J. Geophys. Res. 97 (C7) 11191–11198,

678 https://doi.org/10.1029/92JC00767, 1992.

679

680 Rubino A., Gačić M., Bensi M., Vedrana K., Vlado M., Milena M., Negretti M.E., Sommeria J.,

681 Zanchettin D., Barreto R.V., Ursella L., Cardin V., Civitarese G., Orlić M., Petelin B., and

682 Siena G.: Experimental evidence of long-term oceanic circulation reversals without wind

683 influence in the North Ionian Sea. *Sci Rep* **10 1**905 (2020), https://doi.org/10.1038/s41598-

684 020-57862-6, 2020.

685

686   Schroeder K., Chiggiato J., Josey S., Borghini M., Aracri S., and Sparnocchia S.: Rapid response

687   to climate change in a marginal sea. Scientific Reports. 7, https://doi.org/10.1038/s41598-017-

688   04455-5, 2017.

689

690   Schroeder K.,: Current Systems in the Mediterranean Sea, Editor(s): J. Kirk Cochran, Henry J.

691   Bokuniewicz, Patricia L. Yager, Encyclopedia of Ocean Sciences (Third Edition), Academic

692   Press 2019, Pages 219-227, ISBN 9780128130827, https://doi.org/10.1016/B978-0-12-

693   409548-9.11296-5, 2019.

694

695   Schuckmann K.V., Traon P.-Y.L., Smith N., Pascual A., Djavidnia S., Gattuso J.-P., Grégoire M.,

696   Nolan G., Aaboe S., Aguiar E., et al.: Copernicus marine service ocean state report, issue 3. *J.*

697   *Oper. Oceanogr, 12*, S1–S123, 2019.

698

699   Shaltout M., and Omstedt A.: Recent sea surface temperature trends and future scenarios for the

700   Mediterranean Sea, Oceanologia, Volume 56, Issue 3 2014, Pages 411-443, ISSN 0078-3234,

701   https://doi.org/10.5697/oc.56-3.411, 2014.

702

703   Skliris N.: Past, Present and Future Patterns of the Thermohaline Circulation and Characteristic

704   Water Masses of the Mediterranean Sea. In: Goffredo S., Dubinsky Z. (eds) The

705   Mediterranean Sea. Springer, Dordrecht, https://doi.org/10.1007/978-94-007-6704-1_3, 2014.

706

707   Skliris N., Zika J.D., Herold L., Josey S.A., and Marsh R.: Mediterranean sea water budget long-

708   term trend inferred from salinity observations. *Clim Dyn* **51 2**857–2876 (2018).

709   https://doi.org/10.1007/s00382-017-4053-7, 2018.

710

711   Tsimplis M., Zervakis V., Josey S.A., Peneva E., Struglia M.V., Stanev E., Lionello P.,

712   Malanotte-Rizzoli P., Artale V., Theocharis A., Tragou E., and Oguz T.: Changes in the

713   oceanography of the Mediterranean Sea and their link to climate variability. In: Lionello, P.;

Malanotte-Rizzoli, P.; and Boscolo, R., (eds.) Mediterranean climate variability. Amsterdam, The Netherlands, Elsevier 227-282, 438pp. (Developments in Earth and Environmental Sciences, 4), https://doi.org/10.1016/S1571-9197(06)80007-8, 2006.

Vàrgas-Yáñez M., Moya F., Tel E., García-Martínez M.C., Guerber E., and Bourgeon M.: Warming and salting of the Western Mediterranean during the second half of the XX century: inconsistencies, unknowns and the effect of data processing. Sci. Mar. 73 (1), 7–28, https://doi.org/10.3989/scimar.2009.73n1007, 2009.

Vàrgas-Yáñez M., Moya F., García-Martínez M.C., Tel E., Zunino P., Plaza F., Salat J., Pascual J., López-Jurado J.L., and Serra M.: Climate change in the Western Mediterranean Sea 1900–2008, Journal of Marine Systems, Volume 82, Issue 3 2010, Pages 171-176, ISSN 0924-7963, https://doi.org/10.1016/j.jmarsys.2010.04.013, 2010.

Vàrgas-Yáñez M., Juza M., Balbín R., Velez-Belchí P., García-Martínez M. C., Moya F., and Hernández-Guerra A.: Climatological Hydrographic Properties and Water Mass Transports in the Balearic Channels From Repeated Observations Over 1996–2019, Frontiers in Marine Science, Volume 7, Pages 779, IISN 2296-7745, https://www.frontiersin.org/article/10.3389/fmars.2020.568602, 2020.

Wong A., Keeley R., Carval T., Argo Data Management Team: Argo Quality Control Manual for CTD and Trajectory Data, https://doi.org/10.13155/33951, 2021.

Zu Z., Poulain P.M., and Notarstefano G.: Changes in hydrological properties of the Mediterranean Sea over the last 40 years with focus on the Levantine Intermediate Water and the Atlantic Water, http://maos.inogs.it/pub/Hydro_trend_LIW_SAW_core_report_v10.pdf, 2014.

Table 1. Trends by year for the AW and LIW salinity, temperature, and depth timeseries in eight Mediterranean subbasins. In bold characters the trends significant at 5% level. The rightmost column shows the mean and standard deviation trend values computed over the eight subbasins (here identified with MED). Trends are defined as mean ± standard deviation.

	Algerian	Catalan	Ligurian	Tyrrhenian	Adriatic	Ionian	Cretan	Levantine	MED
Salinity [1/yr]									
AW	**-0.014±0.151**	**-0.004±0.088**	-0.001±0.089	**0.006±0.157**	**0.044±0.188**	**0.009±0.181**	**0.013±0.166**	**0.003±0.100**	**0.007±0.140**
LIW	**0.002±0.022**	**0.002±0.017**	**0.005±0.034**	**0.006±0.035**	**0.021±0.074**	**0.004±0.031**	**0.005±0.048**	**0.004±0.039**	**0.006±0.038**
Temperature [°C/yr]									
AW	**0.054±0.614**	0.019±0.846	0.004±0.914	**0.042±0.528**	**0.117±0.951**	**0.023±0.395**	-0.026±0.786	**0.026±0.683**	**0.026±0.715**
LIW	**0.008±0.125**	**0.010±0.088**	**0.022±0.138**	**0.030±0.167**	**0.093±0.384**	**0.030±0.226**	-0.003±0.226	**0.012±0.391**	**0.022±0.232**
Depth [m/yr]									
AW	**-0.092±2.271**	-0.019±4.646	-0.012±5.720	**0.394±4.002**	0.757±25.800	**-0.324±7.352**	0.116±17.480	**1.087±17.024**	**0.238±10.537**
LIW	-0.352±14.639	**1.895±52.582**	-0.155±40.249	**-7.034±46.395**	2.609±115.404	**-4.973±42.536**	-1.630±26.943	**0.849±32.912**	**1.099±46.458**
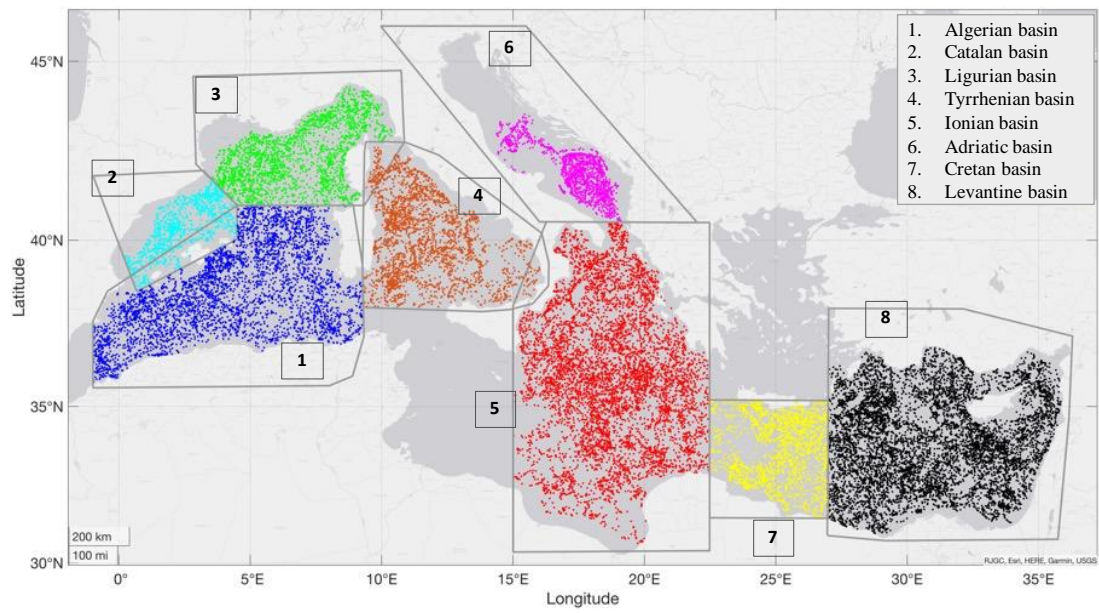
Fig. 1 Argo floats profiles scatter plot in the Mediterranean Sea between 2001 and 2019 in eight regions based on the climatological areas defined by the EU/MEDARMEDATLAS II project.

745
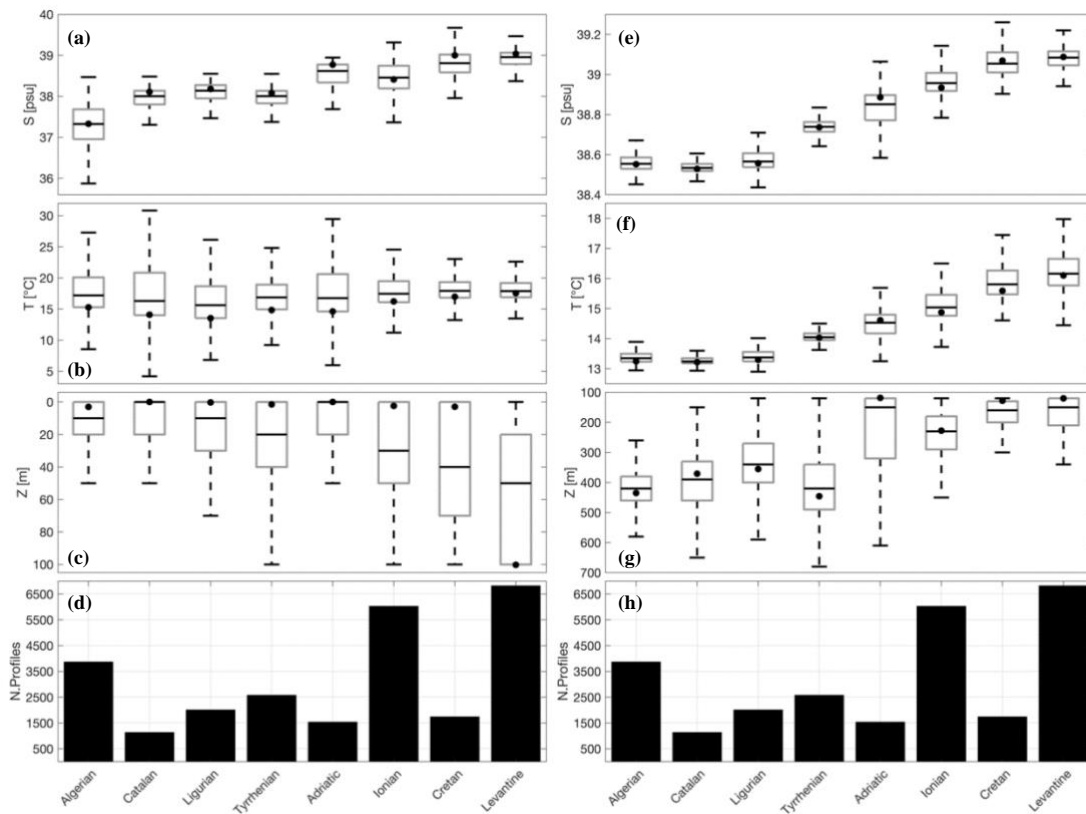
Fig. 2 Boxplot diagrams for the AW salinity (a), temperature (b) and depth (c) in eight

Mediterranean subbasins. Inside each grey box, the black bold line indicates the median, while

the bottom and top edges of the box indicate the 25th and 75th percentiles respectively, and the

black dots show the mode of each distribution, which corresponds to the maximum PDF. The

number of profiles (black bars) for each subbasin are shown in panel (d). The corresponding

diagrams for the LIW are shown in the panels (e,f,g,h).
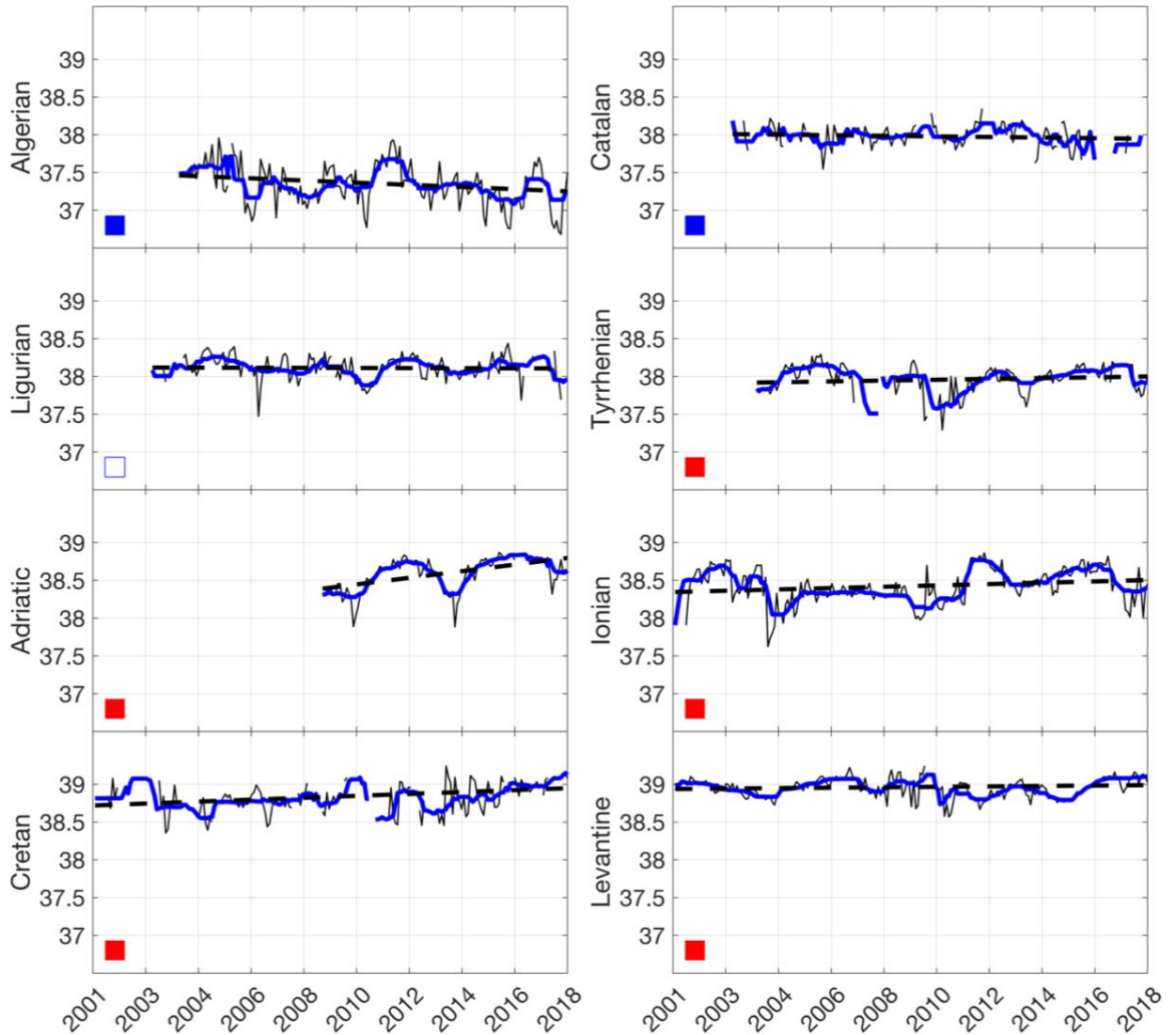
Fig. 3 AW salinity timeseries in eight subbasins: the thin black lines show the monthly timeseries (seasonal cycle filtered out), the tick blue lines are the 1-year moving average timeseries and the dashed black lines are the trends. The red/blue filled squares identify the positive/negative trends with pvalue≤0.05, while the red/blue not-filled squares identify the positive/negative trends with pvalue>0.05.
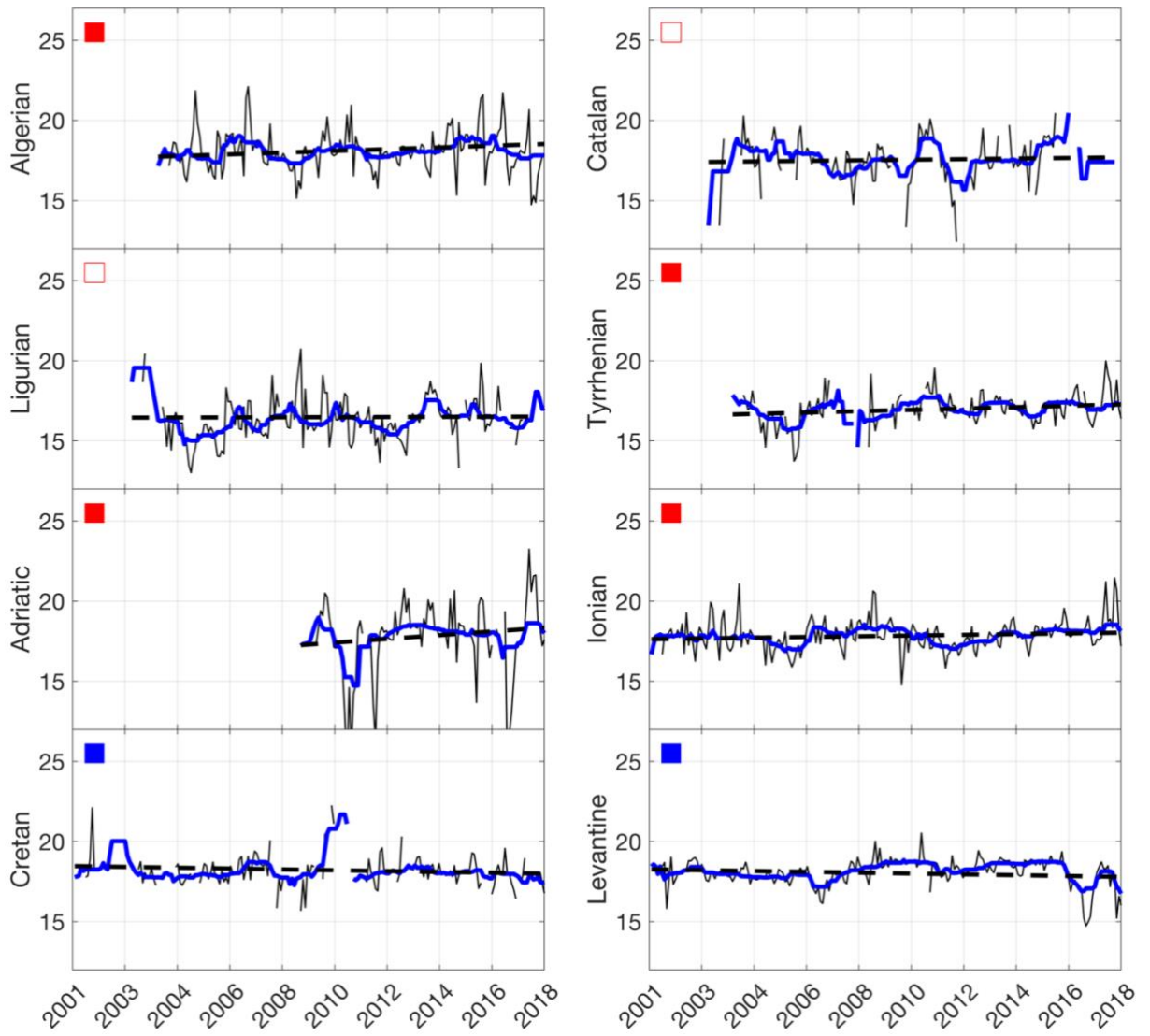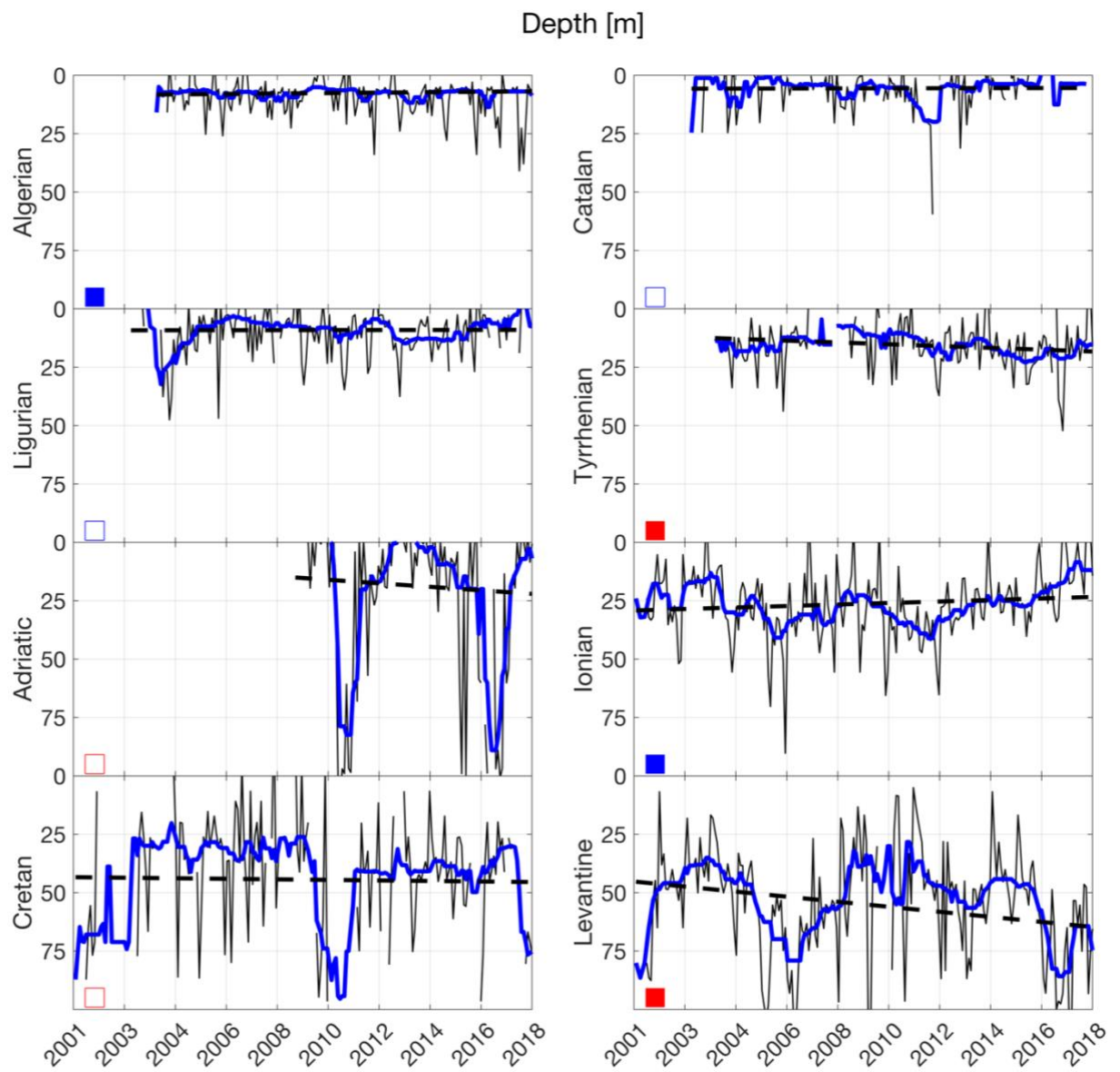
759

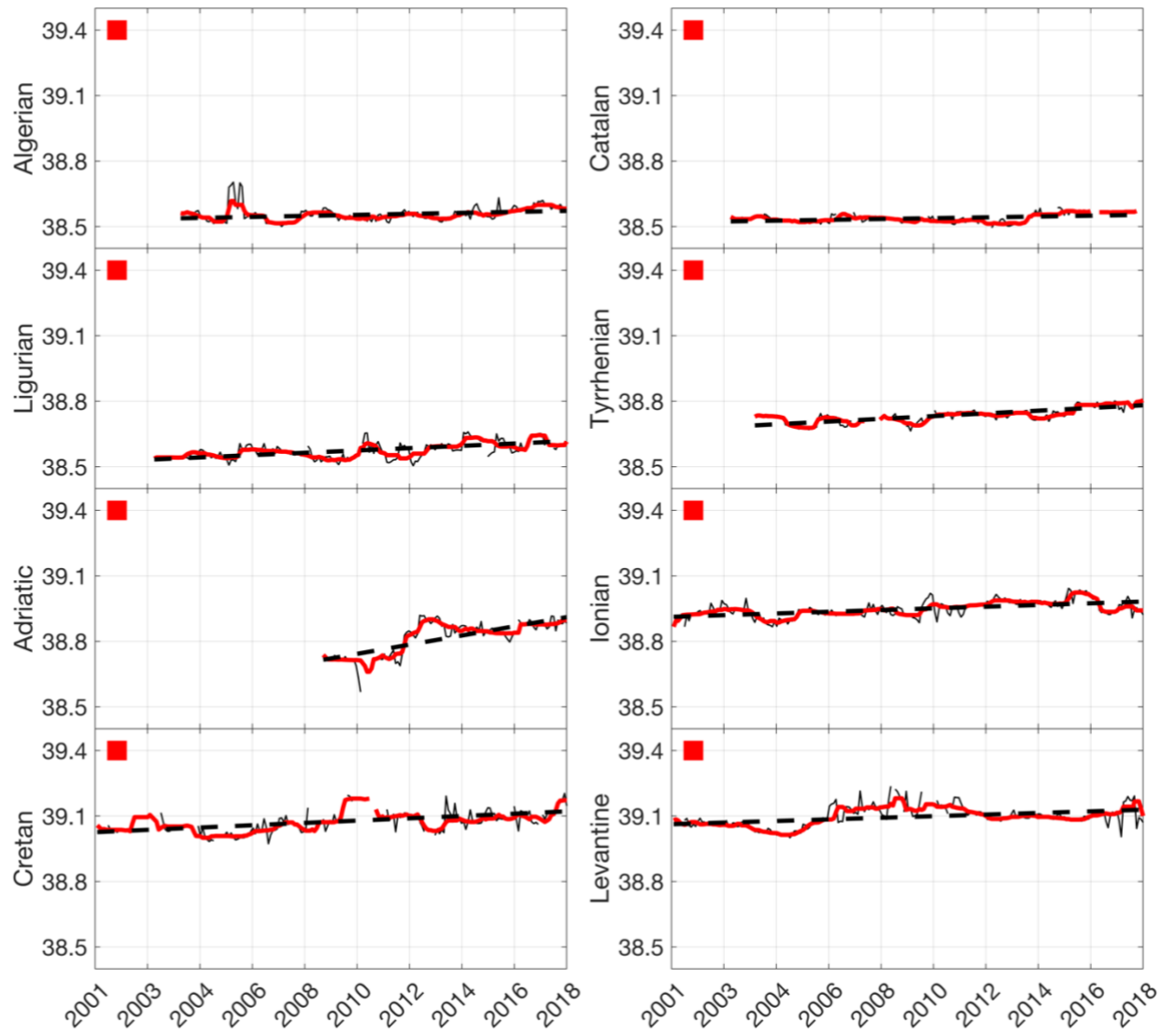760   Fig. 4 Same as Fig. 3 but for the AW temperature.

761

Fig. 5 Same as Fig. 3 but for the AW depth. Positive/negative trends (red/blue squares) in this case corresponds to an increase/decrease of the depth (i.e., deeper/shallower).

766

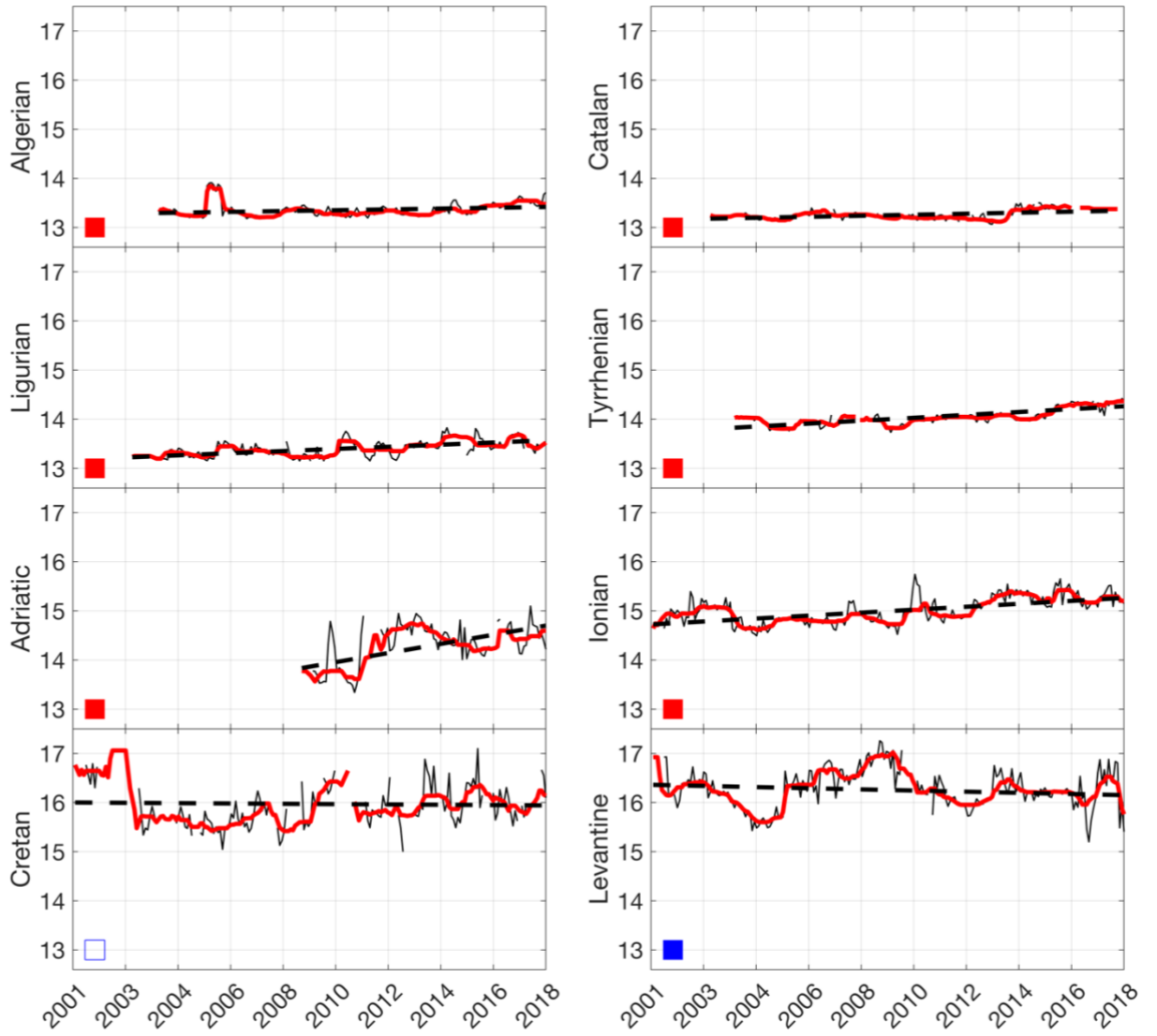767   Fig. 6 Same as Fig. 3 but for the LIW salinity.

768

769

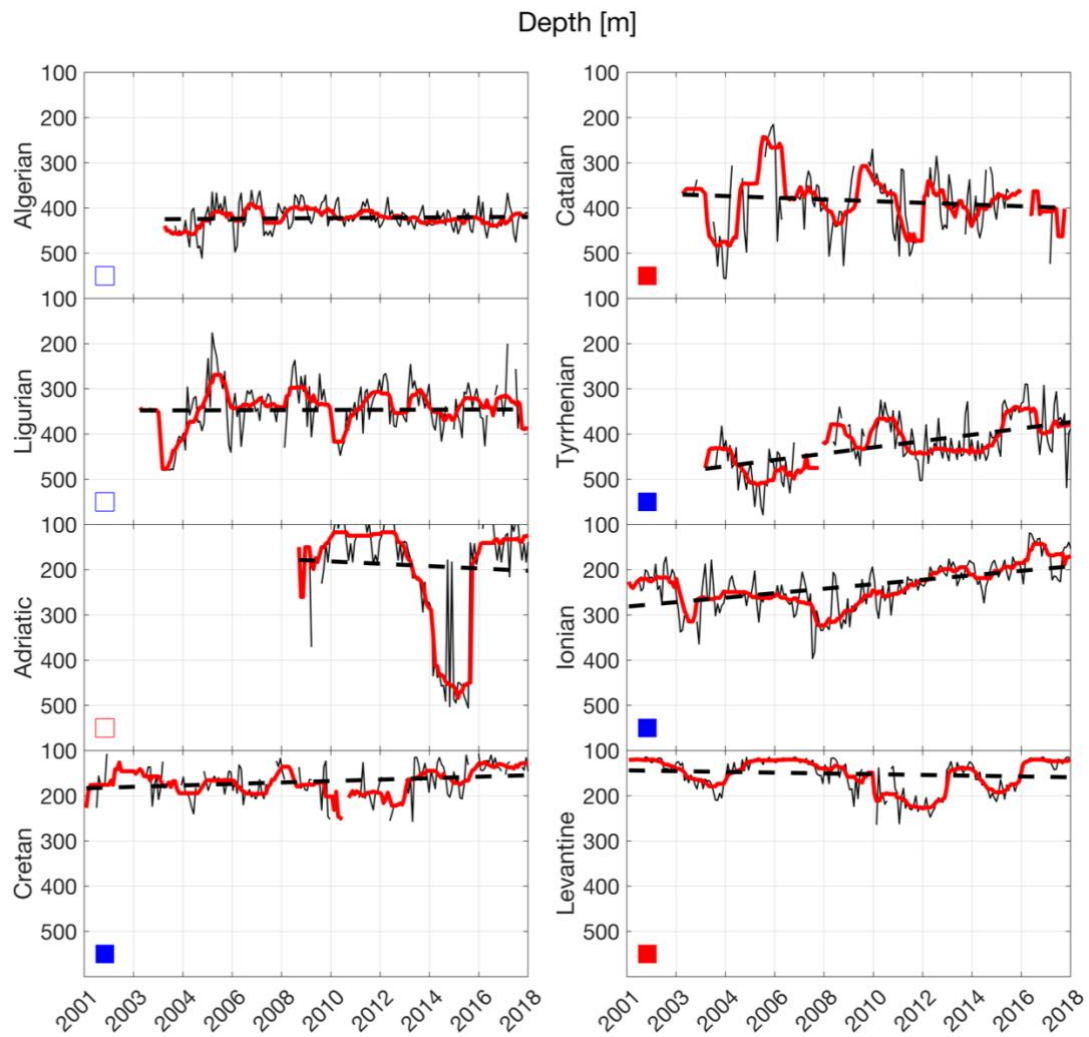770   Fig. 7 Same as Fig. 3 but for the LIW temperature.

771

Fig. 8 Same as Fig. 3 but for the LIW depth. Positive/negative trends (red/blue squares) in this case corresponds to an increase/decrease of the depth (i.e., deeper/shallower).